WELDING RESEARCH

SUPPLEMENT TO THE WELDING JOURNAL, JUNE 1974

Sponsored by the American Welding Society and the Welding Research Council

Flywheel Friction Welding Research

Study reports on thermal behavior, optimization of welds and metallurgy of the bond

BY K. K. WANG AND WEN LIN

ABSTRACT. This paper summarizes the results obtained from a research project on several aspects of flywheel friction welding. Temperature rise at the weld interface is found to be more rapid than that in the continuous-drive friction welding process. In the welding of ⅜ in. diam steel bars, the steepest temperature gradient occurs near the mid-radius in about 0.06 sec. It diminishes in 0.2 sec and reaches a nearly steady state of uniform distribution over the entire interface. An optimum operating condition can be quickly established by applying the Response Surface Methodology. The optimum region for welding low carbon steels is fairly wide.

A retraction experiment on Cu-Al welds indicates that the amount of aluminum adhering to the copper surface first increases and then declines as the time of contact increases. This reflects the fact that the weakest plane on the soft metal side moves away from the interface and then comes back, as determined by the complex interplay between strain hardening and thermal softening. Electron probe microanalyses of the welded joint reveal the existence of intermediate phase(s) at the bond interface. The formation of such alloys is presumably attributed to mechanical mixing and partial diffusion.

K. K. WANG is Associate Professor, Sibley School of Mechanical & Aerospace Engineering, and WEN LIN is Research Manager, Metallography and X-Ray Laboratory, Materials Science Center, Cornell University, Ithaca, New York.

Introduction

Historical Background

It was an old idea to join materials (metals or plastics) together utilizing the heat generated at the interface by friction. Some applications and patents were dated back to the turn of the century (Ref. 1). However, scientific study was not started until 1956 after Chudikov (Ref. 2) had revived the old concept and successfully demonstrated the possibility of achieving high quality butt welds between metal rods. Intensive research effort has been launched since then by Vill (Ref. 3) and others in the U.S.S.R. in order to understand the process from scientific viewpoints. The process was introduced to the U.S.A. in 1960. At the American Machine and Foundry Co., Hollander (Ref. 4) and Cheng (Refs. 5, 6) did some pioneering work on parameter analysis and the thermal aspects of friction welding.

In 1962, Caterpillar Tractor Company developed the so-called inertia welding which is a modified friction welding process employing a flywheel to store the energy required for welding. Since then, the names "conventional" or "continuous-drive" friction welding have been used specifically for the original Russian process; while "inertia" or "flywheel" friction welding have been commonly used for the Caterpillar process. The flywheel process is mostly widely used in the United States.

Although the two processes are basically the same, their thermal and mechanical behaviors are expected to be different due to considerable difference in the rate of energy input to the welding process and in welding cycle time. It is conceivable that these differences may have a significant effect on the metallurgical aspect of the interfacial bond. There has been very little fundamental work published in the literature specifically devoted to flywheel friction welding. This paper

summarizes a few results obtained from a research project partially sponsored by the Welding Research Council dealing with several aspects of the process.

Mechanism of the Process

The principle of flywheel friction welding is illustrated schematically in Fig. 1(a). During welding, one part of the workpiece is held by a chuck or a collet which, along with a replaceable flywheel, is mounted on a rotating spindle. This part is first brought up to a predetermined initial speed of N rpm. To start welding, the other part of the workpiece (nonrotating) is pushed against the rotating part under a constant pressure P, while the driving power is cut off at the mean time. The rotating part is rapidly brought down to standstill by the interfacial friction which generates heat, softens the material, and causes plastic flow and upset. Figure 1(b) shows qualitatively the history of rotating speed, frictional torque, and the amount of upset in a complete welding cycle (Ref. 7).

The mechanism of flywheel friction welding has been characterized by a three-stage model based on the history of frictional torque at the interface (Ref. 8) as shown in Fig. 1(b). Stage I is dominated by the phenomena of dry friction and wear during which interlocking and adhesion of asperities result in a rapid increase of torque to a peak, and concurrently, the whole area is brought into real contact. The power input has its highest value in the same time period because of the large torque and high rubbing speed at this early stage. A large portion of the stored kinetic energy dumped abruptly at the interface disrupts contaminated surface layers and causes softening of the material on the surfaces and initiates thermoplastic flow. Despite the effect of strain hardening, the torque curve drops slightly in the later part of Stage I because of the predominance of thermal softening.

With the nearly instantaneous high power input in Stage I, the plastic flow is essentially confined to a very thin layer at the interface without significant spread into the bulk of the workpiece material. This constitutes the conditions for an adiabatic shear phenomenon (Ref. 9) which characterizes the Stage II mechanism of the welding cycle. The Stage I-II transition period indicates that the process reaches a balance of effects contributed by strain hardening and thermal softening. At this stage the process is self-adjusting and the torque curve remains practically unchanged as shown in the figure. While the speed continues to drop, there is a complex interplay of decreasing power, strain rate, and also temperature such that the balance and relatively constant value of torque is maintained until the Stage II-III transition occurs. At that moment, the temperature gradient across interface is decreasing and the narrow deformation zone is widening rapidly. The adiabatic shear phenomenon diminishes as a result.

Stage III mechanism is dominated by torsional forging as the speed and temperature continue to drop. Gradual stiffening of the material at the weld causes the torque to reach another peak. The amount of upset continues to increase while the material flushes out of the widening heat-affected zone through a spiral path from the center of the interface. Stage III terminates after the rotation is completely stopped and the material at the weld becomes completely rigid.

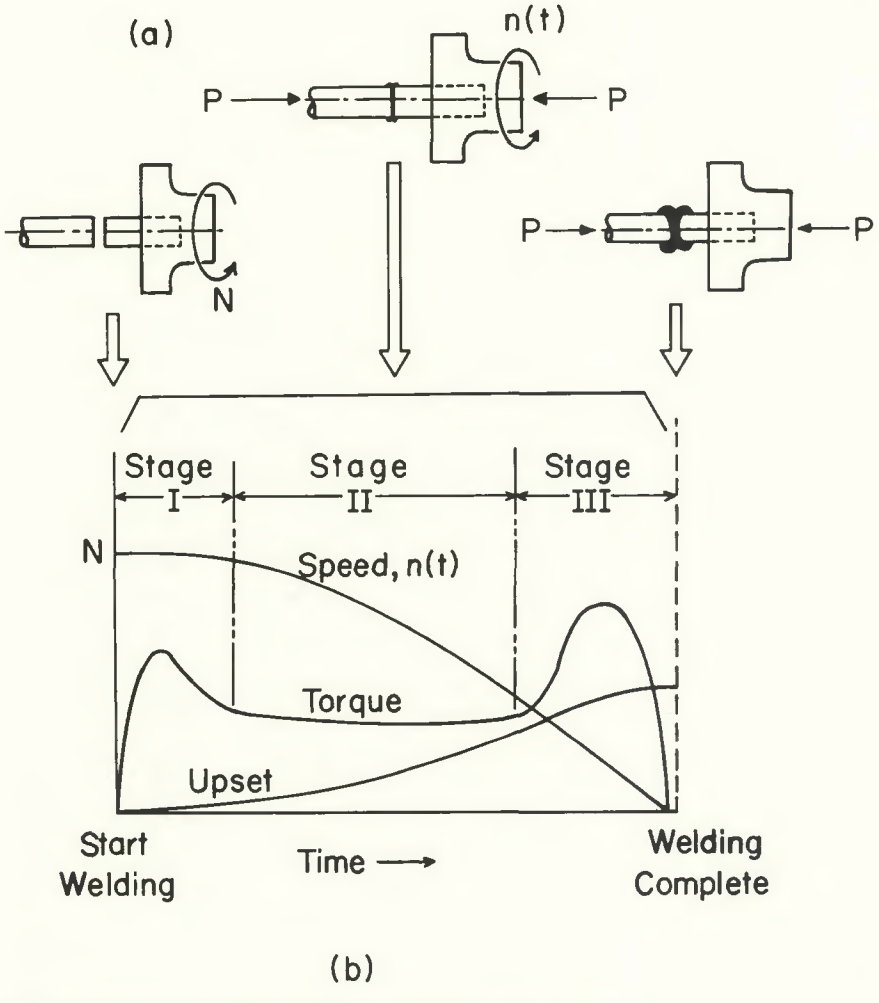

Fig. 1 — Some characteristics of flywheel friction welding process

Objectives of the Research

The study was motivated by the lack of information in the literature with regard to the fundamentals of the flywheel friction welding process specifically. The main objectives of the research are: (1) to investigate the thermal behavior of the process which has much more concentrated power input than the conventional process; (2) to develop a methodology or an experimental procedure so that an optimal weld can be obtained quickly; (3) to study the bonding mechanism at the interface from physical and metallurgical viewpoints.

Thermal behavior of continuous-drive friction welding has been extensively studied through experiments and analyses. Initial controversy over whether melting temperature has been reached at the interface has apparently been resolved. The nature of nearly instantaneous power input in flywheel friction welding is expected to have a significant effect on the thermal behavior of the weld as compared to the relatively lower intensity of power input at longer duration in a typical continuous-drive process. The flywheel process which consists of only three welding parameters is considered relatively easy to be controlled and optimized. An optimization methodology involving sequential procedure of

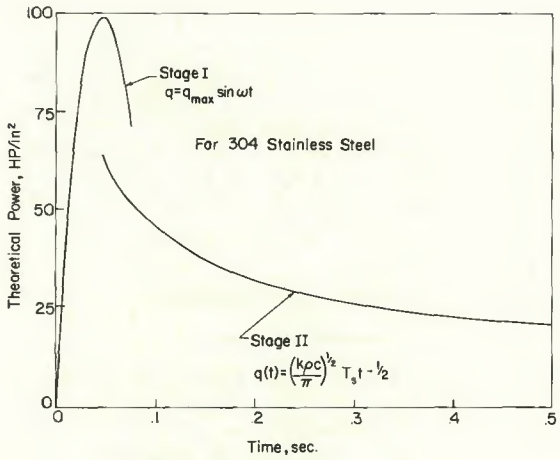

Fig. 2 — Theoretical power input (Ref. 8)

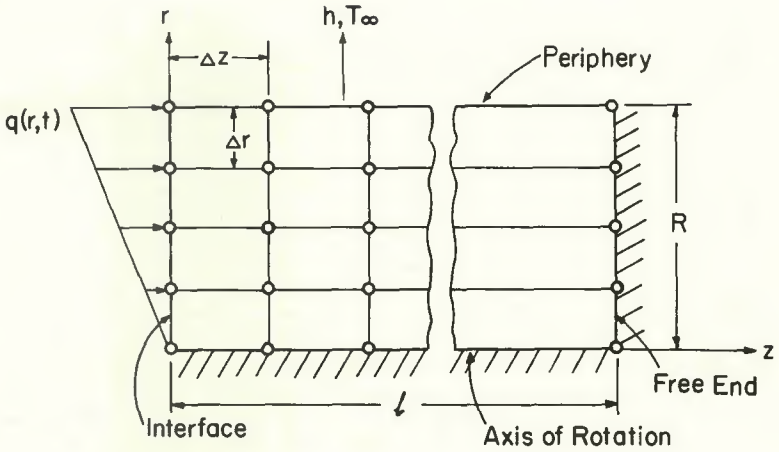

Fig. 3 — Grid network and boundary conditions

experimentation and analysis is established in this study.

Interfacial bonding mechanisms are investigated during Stage I and also after the weld is completed. The result of dry friction and interfacial adhesion which leads to adiabatic shear during the period of Stage I-II transition are studied by examining the metal transfer across the interface after retraction of the workpieces. A mathematical model is established to describe a time function of such metal transfer. Metallurgical examination of the weld zone is concentrated on the possible formation of alloys at the interface. Such investigations were carried out by using metallography and scanning electron microscopy (SEM) techniques.

Thermal Behavior

Power Input

It is conceivable that successful metallurgical bond by friction welding depends much on the thermal behavior at the interface. The transient temperature variation in the weld zone is largely determined by the history of power input during the welding cycle and the thermal properties of the workpiece material. Because of the considerably shorter welding time and more concentrated power input in flywheel friction welding, the temperature distribution is expected to be different from the continuous-drive process. Previous study (Ref. 8) has suggested that theoretical power input at Stages I and II can be represented by the curves plotted in Fig. 2 for 304 stainless welds. The calculations were based on one-dimensional heat flow and constant thermal properties. The linear Stage I power input was approximated by a sine curve. The Stage II power was calculated based on the power required to maintain a surface at some temperature T_s after an instantaneous rise in surface temperature from some lower temperature T_o by the following equation:

$$q(t) = \left(\frac{k\rho c}{\pi}\right)^{1/2} T_s\, t^{-1/2} \qquad (1)$$

It was also reported that the welding cycle time was appreciably affected by the thermal properties of the materials to be welded.

A more rigorous thermal analysis in this study has considered two-dimensional heat flow and temperature-dependent thermal properties of the material. It has been shown (Ref. 10) that the heat input can be expressed as:

$$q(r,t) = 5.8A \cdot r \cdot n(t) \qquad (2)$$

where A is a constant determined by the coefficient of friction and the unit normal pressure, r is the radial distance from the center, and n(t) is the rotational speed as a function of time. This implies that the heat input distribution over the entire interface is proportional to the linear rubbing velocity at a given instant. A typical speed curve exhibits very small change from its initial value in Stage I, and it drops rather rapidly thereafter. A mathematical expression is obtained by fitting a quadratic equation to a recorded speed curve so that the equation can be used in the calculation of power input.

Transient Temperature Distribution

An analysis of temperature variation has been carried out in this study for a steel to steel weld of round bars. Due to the rotational symmetry, the differential equation for two-dimensional unsteady heat flow in solids is given by:

$$\frac{\partial^2 T}{\partial r^2} + \frac{1}{r}\frac{\partial T}{\partial r} + \frac{\partial^2 T}{\partial z^2} = \frac{1}{\alpha}\frac{\partial T}{\partial t} \qquad (3)$$

Since the thermal properties of low carbon steel vary widely and irregularly with temperature within the working range of the welding process, Eq. (3) becomes a nonlinear partial differential equation for which an exact analytical solution is not readily available. Therefore, the thermal analysis is performed by numerical methods using a digital computer. Figure 3 which shows a half section of the workpiece is the grid network employed in the finite difference approximation with boundary conditions specified. The heat input q(r,t) from Eq. (2) is taken as surface heat flux flowing into the nodes at the interface. Heat loss through the peripheral surface of the workpiece by convection is calculated based on the condition of a rotating horizontal cylinder in still air with a variable coefficient of convection h and an ambient temperature T_∞. No heat flow is expected across the centerline because of the rotational symmetry. It is assumed that there is no heat transfer at the far end of the workpiece since little temperature rise has been noticed there during the welding cycle.

With these boundary conditions and using a forward step finite difference method, the difference equation for the nodal points at the interface is

$$T_{i,1}^{t+1} = T_{i,1}^{t} + \frac{\alpha\Delta t}{(\Delta r)^2}\left[\left(\frac{9-2i}{10-2i}\right)T_{i-1,1}^{t} + \left(\frac{11-2i}{10-2i}\right)T_{i+1,1}^{t} - 2T_{i,1}^{t}\right] \qquad (4)$$

$$+ \frac{2\alpha\Delta t}{(\Delta z)^2}\left[T_{i,2}^{t} + \frac{q\Delta z}{12k} - 2T_{i,1}^{t}\right]$$

where q is the heat flux flowing into a node as calculated by Eq. (2). The difference equation for the nodes on the peripheral surface will include a term of convection heat loss while the equation for all interior nodes involves no heat transfer from exterior

sources or to the surroundings. The time interval Δt is chosen at 0.001 sec to fulfill the stability criterion for convergence in the calculation.

In computation, the temperature-dependent thermal diffusivity of the material is updated in each iteration cycle according to the property curve. The computed temperatures for the nodes near interface are further modified after each time interval by taking into account the amount of upset. The total amount of upset measured from the experiment is equally distributed to the two sides of the workpiece with linear variation with respect to time. The modified temperatures at the new interface were then calculated by linear interpolation based on temperatures of adjacent nodes. Temperatures at several interior locations were also measured experimentally for verification purposes. This has been done by inserting fine thermocouples into the bottom of several drilled holes at various locations.

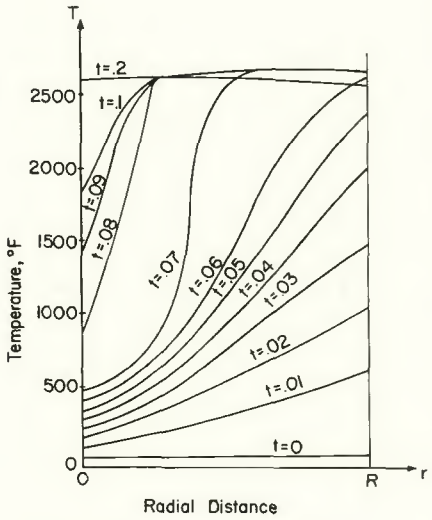

Fig. 4 — Transient temperature gradients at the interface

Figure 4 shows the computed transient temperature distribution at the interface when the low carbon steel rods of 3/8 in. diam were welded. The temperature at the periphery of the interface increases rapidly to a maximum value approaching the melting point in 0.060 sec. The steepest temperature gradient occurs at about the mid-radius. Through heat conduction, it reaches a nearly uniform distribution in about 0.2 sec. The temperature gradient on the surface in the longitudinal direction of the workpiece is shown in Fig. 5. It can be seen that the highest temperature is attained at the outermost portion of interface in a very early stage of the welding cycle. This temperature tapers off slightly when time goes on because of heat flow through conduction. Also noted is that temperature rise at the location only 3/8 in. away from the interface is rather small at the end of the welding cycle. This indicates that high thermal gradient exists on the periphery of the workpiece during welding. Such temperature gradient, however, will diminish quickly when heat is further dissipated into the bulk of the material after welding is completed.

Another interesting observation according to the theoretical model is the effect of total welding time on peak temperature and temperature variation. Figure 6 indicates that prolonged welding cycle time will reduce the peak temperature necessary to achieve a successful weld. The welding cycle time is primarily determined by the process parameters and the thermal properties of the materials.

Process optimization

Optimization Strategy

The flywheel friction welding process has three controllable parameters which dictate the quality of the weld. They are the thrust pressure, the initial rotating speed, and the moment of inertia. The latter two parameters determine the amount of kinetic energy available for the process and the thrust pressure affects the welding cycle time. Since each parameter has a wide range of variation and many dissimilar metal welds are very sensitive to parameter settings, it is essential to perform welding at optimum conditions before one can start investigating the nature of a bond. Determination of such parameter values has been primarily dependent on experience attained through hundreds of experimental runs. It has been found that each metal pair and each design of joint configuration has its own peculiar range of optimum parameter levels. As a result, considerable effort is usually needed to arrive at an optimal operating condition for a new pair of metals or a new design of weld joint.

Lack of theoretical functional rela-

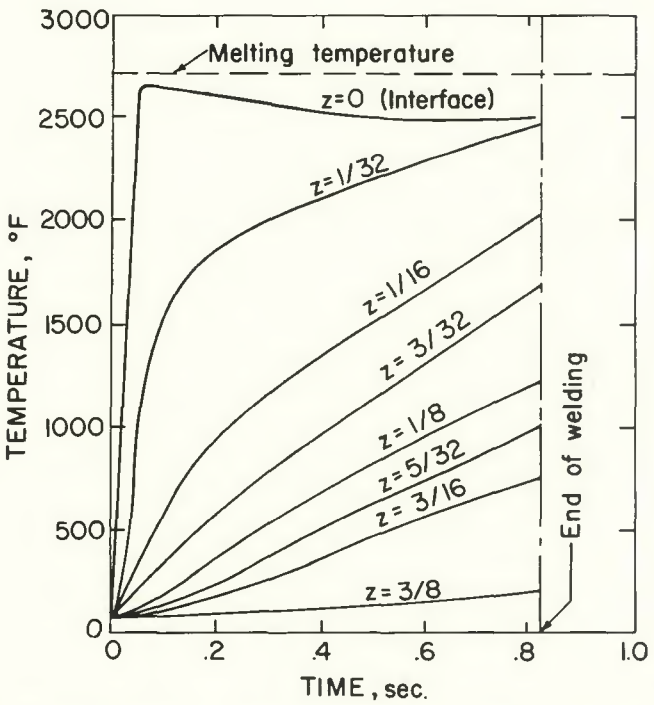

Fig. 5 — Temperature variation on the periphery of the workpiece

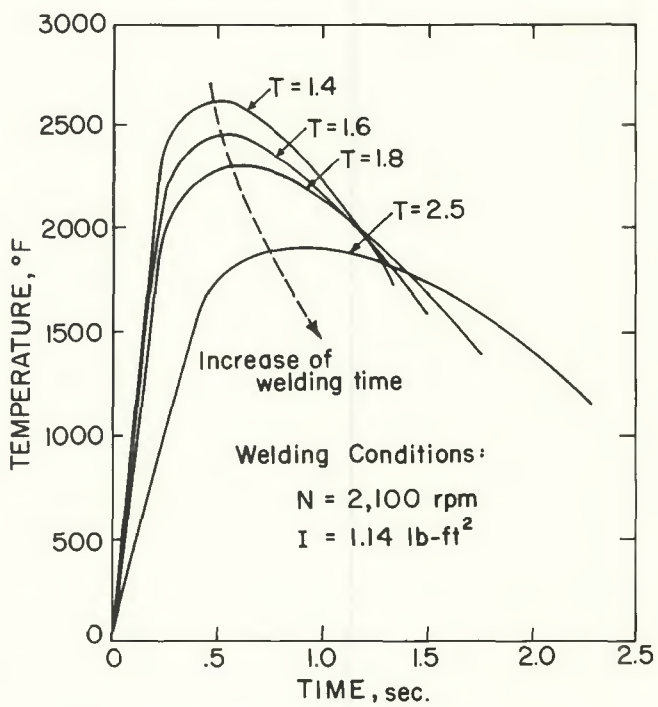

Fig. 6 — Effect of welding cycle time

tionship between weld quality (e.g., weld strength) and process parameters makes it necessary to use an empirical approach. The Response Surface Methodology (Ref. 11), a powerful optimization technique, is applied in this study. The basic idea of this optimization scheme is to explore an unknown response surface which is assumed regionally continuous and smooth by design of experiments. Successive applications of steepest ascent technique will bring the experiments quickly to a near-stationary region which could contain a true maximum. Then, more detailed experiments in this limited region will determine the local nature of the surface. In the study of low carbon steel friction welds, the optimum region is reached in three steps (Ref. 12). A response surface equation is established to represent the characteristics in this region. It is a three-dimensional quadratic equation of the following form after canonical reduction:

$$Y = 105.146 - 1.980\ X_1^2 - 0.545\ X_2^2 - 0.319\ X_3^2 \quad (5)$$

where Y represents the breaking strength of the weld in ksi; X_1, X_2, and X_3 are transformed variables for the thrust pressure, initial speed, and the moment of inertia respectively.

Equation (5) represents a family of ellipsoids centered at the optimum point as shown in Fig. 7 in half of the sections. Each ellipsoidal shell represents the locus of a constant breaking strength Y. The three shells shown in the figure are, from inside out, response surfaces for breaking strengths of 103, 100, and 90 ksi, respectively. The equation as well as the graph clearly indicate that the weld strength decreases from the maximum value at a faster rate along the X_1 direction than the other two directions. It is also noted that the rate of change in response to the optimum region is rather small. This implies that friction welding of low carbon steels allows a relatively wide range of parameter combinations within which weld strength of more than 100 ksi can be obtained.

The Optimum Weld

In addition to the tensile test of breaking strength of the weld, metallurgical examination has been carried out to assess the properties at the weld. Figure 8 shows a macroscopic view of a sectioned specimen made under the optimum condition. The rows of white spots are microhardness indentations to study the distribution of hardness at the weld. The contaminated surface layers which have been first disrupted and squeezed out of the interface area are barely visible as a light gray shade in the mushroom portion of the figure. The microstructure in this region is characterized by elongated coarse grains with plenty of inclusions of oxides and voids. The darker feather-shaped part along the center portion of the weld is the fresh subsurface material being flushed out during the forging stage. Its microstructure is dominated by severely deformed grains with outer portions partially recrystallized.

Figure 9 is a photomicrograph showing typical microstructure in the transition zone near the center of the weld. The orientation of elongated ferrite and pearlite grains exhibits the direction of plastic flow. The subsurface material flows outward in a spiral path due to the combined normal and shear stresses during the forging stage of the welding cycle. The partially deformed heat-affected zone is shown in two bright strips around the weld as viewed in the lightly etched macrograph in Fig. 8.

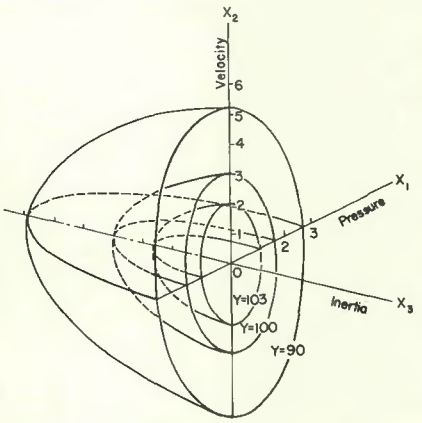

Fig. 7 — Response surfaces representing weld strengths as a function of welding parameters

The microstructural change of material at the weld due to mechanical and thermal effects of the welding process is reflected in the distribution of microhardness measurements. Figure 10 shows the microhardness distribution on one quarter of a sectioned specimen. The average Knoop Hardness Number of the base metal is 213. There is a substantial increase in hardness from the base metal to the interface and from the periphery to the center of the specimen. The highest hardness which occurs around the center portion of the inter-

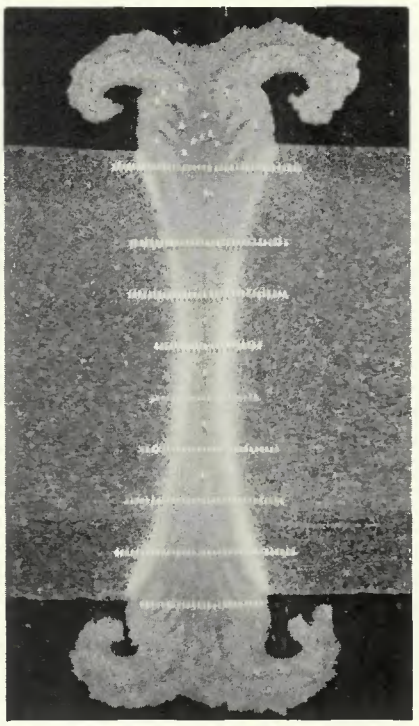

Fig. 8 — Macrograph of a low carbon steel weld

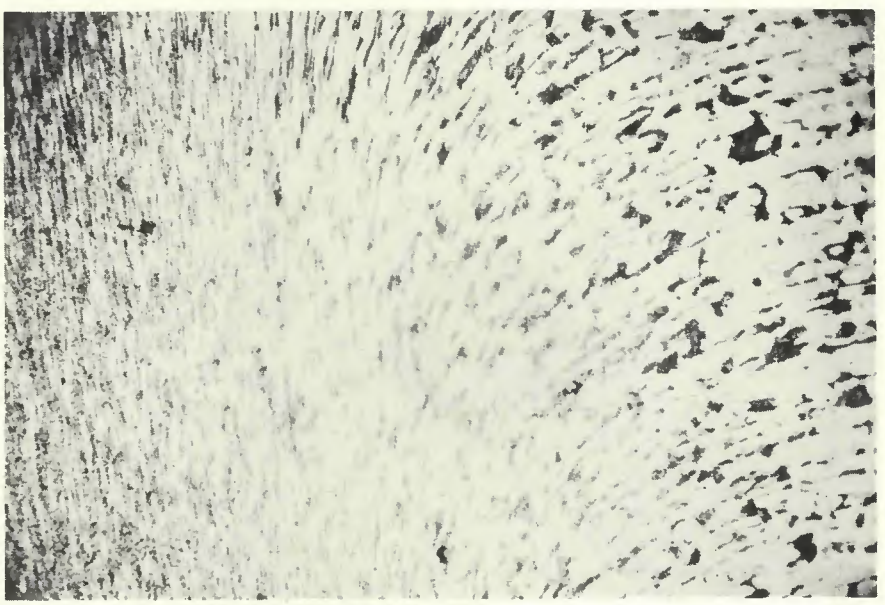

Fig. 9 — Photomicrograph of the transition zone. Etched; X400, reduced 31%

face is averaged to 281, a 32% increase over the base metal. In the shaded region of Fig. 10, however, the hardness decreases to 177, or 17% below the base metal. This is attributed to the grain growth (as evidenced by the microstructure) caused by persistent higher rate of heat input to the outer portion of the specimen, thus, this part of the material stays in high temperature longer than elsewhere. It is apparent, therefore, that an ideal weld should be made with least possible amount of kinetic energy as long as complete bond and full penetration at the interface are achieved. The specimen shown in Fig. 8 appears to have accomplished that requirement. The average Knoop Hardness Number across the interface is 270 or about 27% higher than the base metal. This agrees approximately with an average increase of 24% in breaking strength at the weld as obtained by tensile test.

For welding a new pair of dissimilar metals without prior experience, it is conceivable that more steps may be needed to attain the optimum condition. Nevertheless, the Response Surface Methodology used in this study has demonstrated its effectiveness in dealing with this type of problem.

Bonding Mechanisms

A Metal Transfer Model for Stage I

As described earlier, Stage I of the welding cycle is characterized by the mechanism of dry friction and wear under severe pressure and rubbing speed. The interfacial frictional torque first reaches a peak and then slightly drops off when the two surfaces are in complete contact and the adiabatic shear state is established. To investigate what is happening at the interface during this stage which lasts only a small fraction of a second is a rather difficult task. In this study, a retraction experiment has been carried out to see how the material would be transferred by adhesion from one side to the other after the workpieces are forced to separate (Ref. 13). The retraction is done after they have been in contact for a predetermined length of time. Disruption and adhesion of surface asperities cause some of the soft material to be welded on the surface of the hard material even after they are brought apart again.

In this study a precision analytic balance with a resolution of 10^{-4} g is used for weight measurement. The materials are OFHC copper and 1100-0 aluminum bars of 3/8 in. diam. The specimens before weld were thoroughly cleaned and carefully weighed. Possible metal transfer between the soft workpiece materials and the hard steel holding chucks has been checked and found to be insignificant. Wide range of thrust pressure and initial speed has been selected in the experiment with the moment of inertia of 1.4 lb-ft^2 remaining unchanged throughout. The length of contact was measured in terms of the number of revolutions as the two surfaces are in actual con-

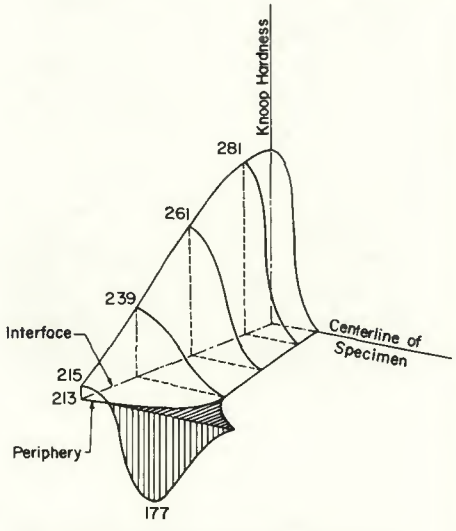

Fig. 10 — Distribution of microhardness

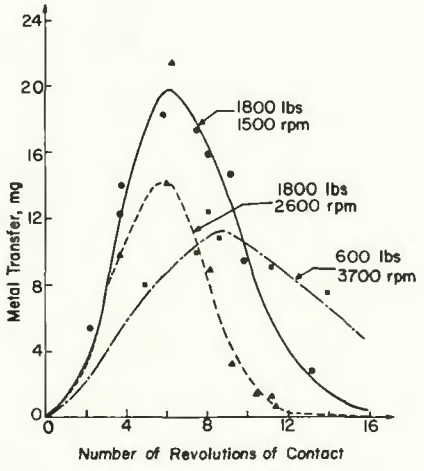

Fig. 11 — Metal transfer model of Cu-Al welds

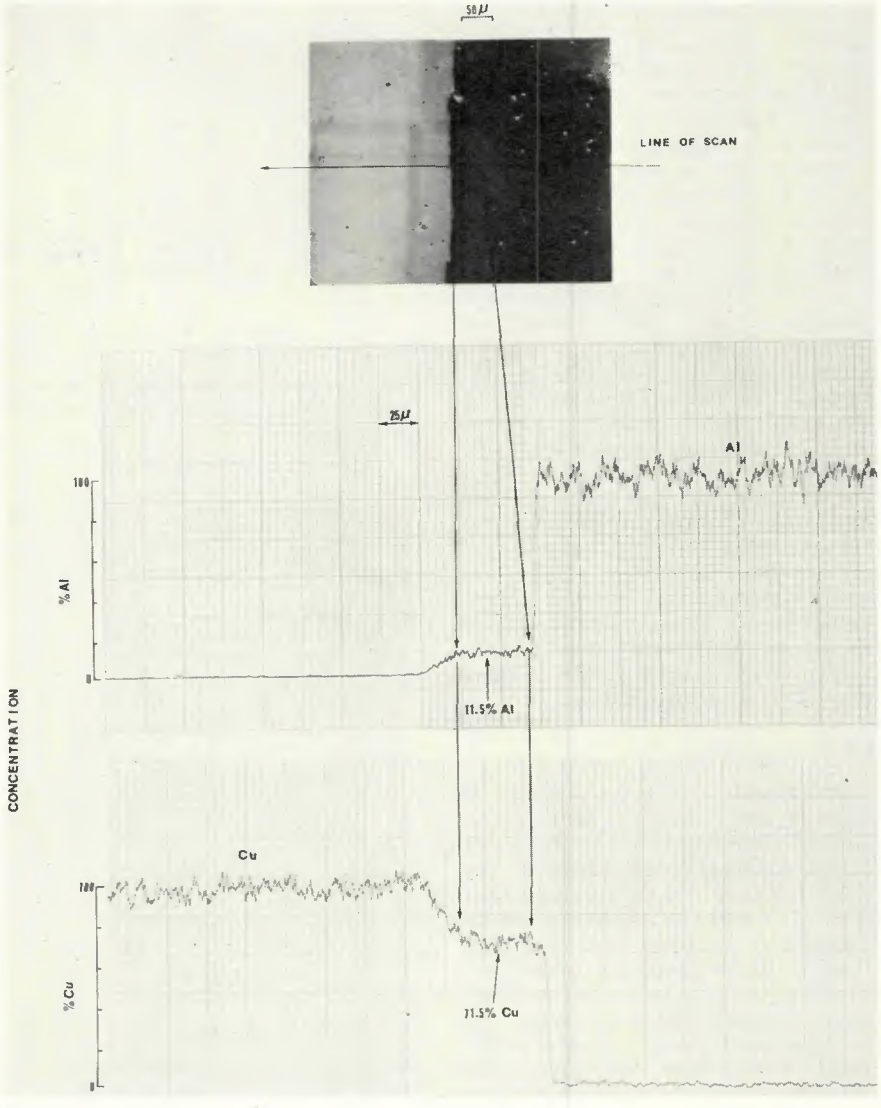

Fig. 12 — SEM image and concentration profiles of Cu-Al weld (center portion)

tact. A predetermined number of revolutions is set by a 3 digit thumbwheel digital switch. Actual number of revolutions is monitored by a digital counter through a magnetic pickup. A digital control device is built to trigger the separation of the workpieces when the preset number of revolutions is obtained.

Figure 11 shows a few typical metal transfer curves for copper-aluminum welds at different welding conditions. In every case the amount of aluminum welded onto the copper surface after retraction first increases and then drops off. This type of curve can often be observed in many rate processes of chemical reaction. Therefore, a basic single-variable model of the following form is first entertained:

$$y = a\, x^{b} \exp(-cx^{d}) \qquad (6)$$

where a, b, c, d are constants. Equation (6) consists of two parts. The power function x^b dominates the process characteristics of the early stage while the exponentially decaying function is responsible for the behavior of the later portion of the process. The constants (or parameters), coefficients and exponents, are estimated using nonlinear least squares method. A statistical model-building method (Ref. 14) is applied to refine the tentative model through an iterative process. The basic ideal of this method is that constants in the model should remain constant and not affected by the change of settings of the variables if the model is correct. Should a parameter be found not a constant but a function of the independent variables, the model can be refined with its new parameters estimated. This procedure is carried on until the condition that constants remain constant is reasonably met.

Following this method and taking all three variables into consideration, a metal-transfer model for copper-aluminum welds is given by the following complex form:

$$W = \frac{0.348\, P^{0.74} S^{0.51} L^{(1.42+0.62P-0.017PS)}}{\exp(0.0023 P^{1.43} S^{0.376} L^{2.43})} \qquad (7)$$

Where W is the weight of metal transferred in mg; P is the thrust force in kips; S is the initial speed in rpm; and L is the sliding distance in inches. For given values of P and S, the metal transfer as a function of L will be represented by the curves in Fig. 11.

Characteristics of Interfacial Bond

In welding of dissimilar metals, layers of various alloys may be formed at the bond interface. The nature of the alloy formed depends on the welding condition and chemical elements of the materials involved.

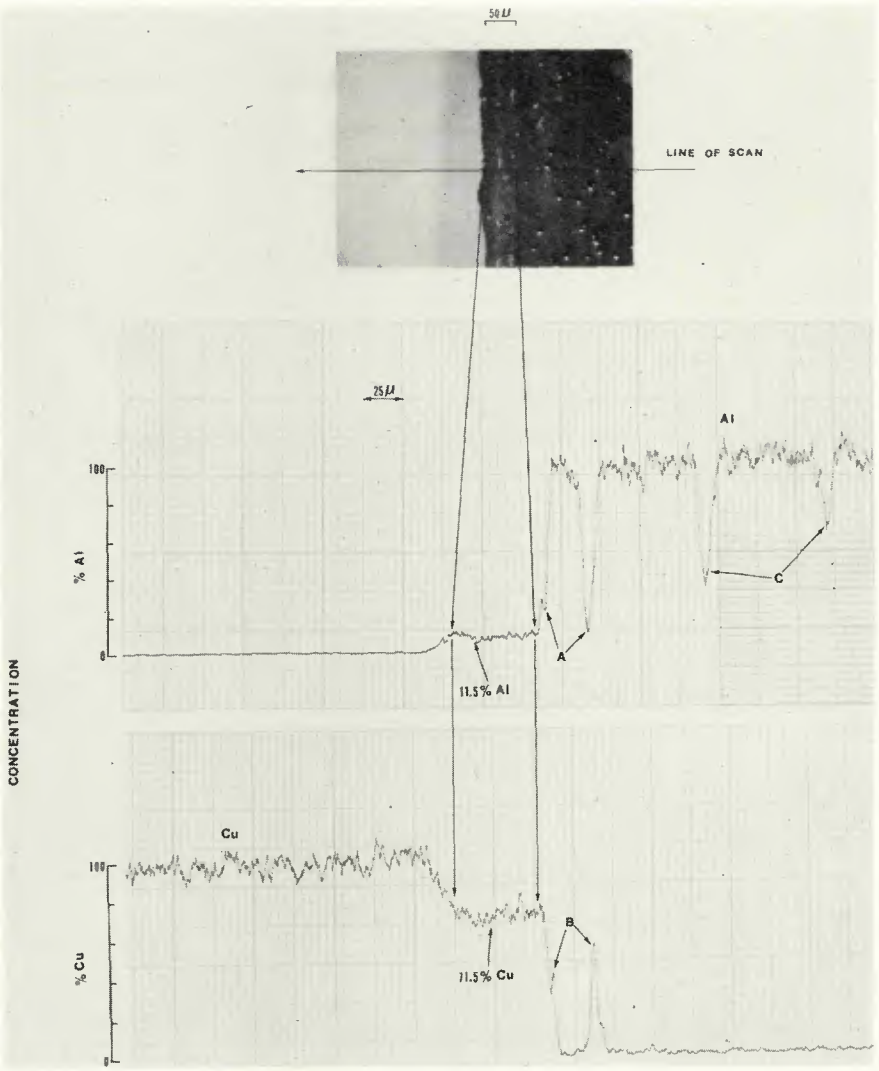

Fig. 13 — SEM image and concentration profiles of Cu-Al weld (at mid-radius)

By studying the element distributions across the weld, it is possible to infer and better understand the nature of the bond. The electron probe microanalysis is an ideal tool for this purpose. In the present study, aluminum-copper and aluminum-stainless steel welds were investigated. In the aluminum-copper weld, 1100-0 aluminum and OFHC copper rods were used. 6061-T651 aluminum and 303 stainless steel were used in the aluminum-stainless steel weld. The longitudinal cross sections containing the center of the weld were cut for the specimen. All specimens were metallographically polished. Care was taken during the specimen preparation to avoid the "smearing" of the base metals across the interface. Only aluminum etch was applied to the aluminum-stainless steel joint.

The electron probe microanalyses were performed on an AMR 900 scanning electron microscope (SEM), which has been modified to include a slow line scan generator for spots with variable scan rate. The effective spot size is about 1 micron in diameter. The excited characteristic x-rays were collected using a Si(Li) solid state energy dispersive detector. Amplified signals for all x-rays can be stored and displayed simultaneously in a multichannel energy analyzer. In this way, a rapid qualitative element analysis may be performed.

If a pulse height analyzer (PHA) is used for the amplified signals, with a proper setting of the PHA, only the selected characteristic x-ray energy will be recorded in the multichannel analyzer and simultaneously on a rate meter-chart recorder system. The characteristic K_α radiations excited from a specific element can thus be recorded as a function of position of electron beam spot as it scans perpendicularly across the weld interface. An acceleration voltage of 21 kV for the electron beam and a take-off angle of 30 deg were used for all scans.

Figure 12 shows a SEM image of the center of an aluminum-copper weld. The aluminum and copper concentration profiles across the weld are shown in the upper and lower

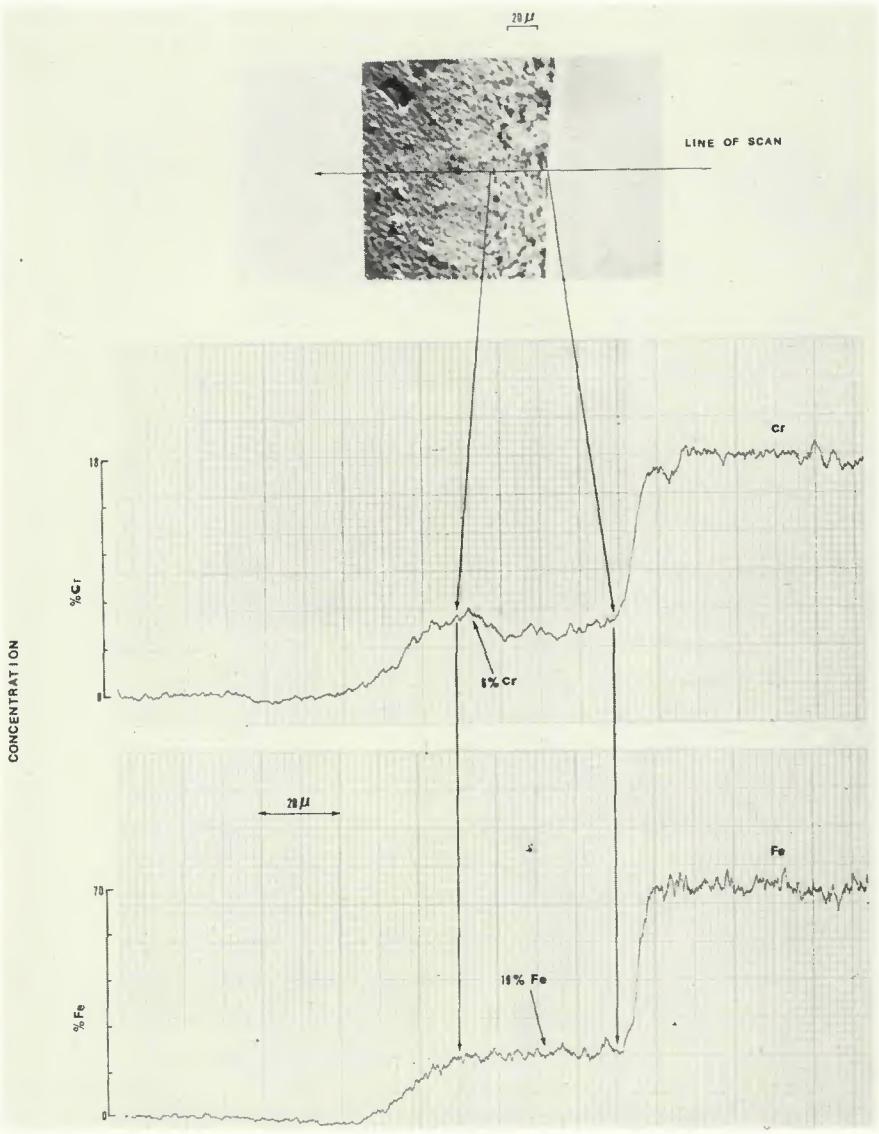

Fig. 14 — SEM image of aluminum-stainless steel weld (center portion)

charts, respectively. Clearly, the concentration changes are not continuous; instead, a range of discrete composition is observed in the immediate vicinity of the "apparent boundary", towards the aluminum side. This range is about 50 microns. The concentration indicated is the "observed" value, which is simply the ratio of the measured intensity to that of the pure metal. Since the elements aluminum and copper are widely separated in atomic numbers, the excited Al K_α radiation from the Al-Cu alloy is highly absorbed by copper in addition to self absorption. The measured Al K_α intensity is substantially lower than the true intensity and it is subjected to correction.

A composition of 26.5% Al and 72.8% Cu was obtained after the absorption correction, following the method described by Phillibert (Ref. 15). This composition corresponds to an aluminum-copper solid solution (ξ_2) with monoclinic crystal structure below 500 C (Ref. 16). Since the composition range of this solid solution is fairly narrow (less than 2 wt %), it is conceivable that there may be some neighboring phase present (about 4 wt % difference). If this were the case, we would expect small deviation in intensity due to the presence of the second phase. It is estimated that this deviation is within the intensity fluctuation about the mean due to counting statistics. Taking into consideration the scan rate used and the small but highly elongated grains formed at the bond, it is possible that this layer contains small amounts of the second phase with the majority of them being ξ_2 phase. It seems reasonable that the formation of the intermediate phase (or phases) primarily results from the mechanical rubbing and mixing action of two dissimilar metals under high pressure and temperature. It is difficult to infer just how much the intermetallic diffusion process has contributed to the alloy formation.

Attempts have been made in order to identify this intermediate phase using transmission x-ray diffraction from the edge of a wedge shaped specimen containing a part of the weld interface. Unfortunately, only the diffraction lines from the base metals were detected. This result is not surprising since the alloy layer is less than 50 microns in thickness. Diffractions from this small mass are easily masked by the diffraction effects due to the neighboring base metal.

Figure 13 shows a region of the aluminum-copper weld at the midpoint between center and periphery. The corresponding concentration profiles are also shown. A layer of intermediate composition similar to that shown in Fig. 12 is observed. However, there appear to be several sharp discontinuities in both aluminum and copper profiles on the aluminum side. Dips of type "A" in aluminum profile and corresponding peaks in copper profile are likely due to the possibility that fine copper particles may have been torn off from the surface of the copper and spread over here and there in the aluminum workpiece. This phenomenon seems to be more pronounced at the position where higher rubbing velocity takes place. This is evidenced in Fig. 13, while it is not observed in Fig. 12. Dips of type "C" observed in the aluminum profile could result from some contaminations or deep microcracks.

In the case of the aluminum-stainless steel weld, one would expect a more complex situation simply because there are more elements involved. Formation of binary or ternary alloys is possible from major constituents, i.e., aluminum, iron, chromium and nickel. The K_α radiations excited from these elements are subjected to extensive absorption and matrix enhancement effects. A detailed analysis is a more difficult task. No effort has been made towards correction. Figure 14 shows a SEM image of the center of the aluminum-stainless steel weld and corresponding concentration profiles. The scan rate used was 0.6 microns/sec. Sharp drops in iron and chromium concentrations occur near the apparent boundary, and it is followed by a zone of intermediate composition of 40-50 microns in thickness. Judging from these profiles one tends to conclude that a ternary alloy is formed at the joint which contains aluminum, iron, chromium and perhaps some minor elements such as nickel and molybdenum.

Conclusions

1. The transient temperature variation in flywheel friction welding is dis-

tinctively different from the continuous-drive process. In welding mild steel bars of 3/8 in. diam, the steepest temperature gradient occurs near the mid-radius in about 0.06 sec. A nearly steady state of uniform temperature distribution over the entire interface is reached in only 0.2 sec.

2. An optimum welding condition can be quickly established by the application of Response Surface Methodology. Welding of mild steels allows a fairly wide region for selecting welding parameters to yield optimum results.

3. The retraction experiment of Al-Cu welds indicates that the amount of aluminum adhering to the copper surface first increases and then declines as the time of contact increases. This reflects the fact that the weakest plane on the soft metal side shifts away from the interface and then moves back, as determined by the complex interplay between strain hardening and thermal softening.

4. Electron probe microanalyses by SEM indicate that an intermediate phase or phases at the bond interface are in existence. Formation of such alloys is presumably attributed to mechanical mixing and partial diffusion.

Acknowledgements

The authors wish to express their sincere appreciation to the Welding Research Council for partial financial support of the project, and to the Caterpillar Tractor Company for the donation of a research flywheel friction welding machine which makes a number of experiments possible.

References

1. Crossland, B., "Friction Welding", Contemporary Physics, Vol. 12, No. 6, Nov. 1971, pp. 559-574.

2. Quimby, J. A., "Friction Welding, Past-Present-Future", ASTME Creative Mfg. Seminar, Technical Paper No. SP65-90, April 1965.

3. Vill, V. I., *"Friction Welding of Metals"*, translated and published by the American Welding Society, 1962.

4. Hollander, M. B., Cheng, C. J. and Wyman, J. C., "Friction Welding Parameter Analysis", *Welding Journal*, Vol. 42 (11) Nov. 1963, Research Suppl., pp. 495-s to 511-s.

5. Cheng, C. J., "Transient Temperature Distribution During Friction Welding of Two Similar Materials in Tubular Form", *Welding Journal*, Vol. 41 (12) Dec. 1962, Research Suppl., pp. 542-s to 550-s.

6. Cheng, C. J., "Transient Temperature Distribution During Friction Welding of Two Dissimilar Materials in Tubular Form", *Welding Journal*, Vol. 42, No. 5, May 1963, Research Suppl., pp. 233-s to 240-s.

7. Oberle, T. L., Loyd, C. D., and Calton, M. R., "Caterpillar's Inertia Welding Process", SAE Trans., Sec. 3, Vol. 75, 1967, pp. 28-35.

8. Caterpillar Tractor Company, "Inertia Welding", *unpublished technical report*, Nov. 1966.

9. Chin, G. Y., Hosford, W. F., and Backofen, W. A., "Influence of Mechanical Loading System on Low-Temperature Plastic Instability", Trans. AIME, Vol. 230, Aug. 1964, pp. 1043-1048.

10. Wang, K. K., and Nagappan, P., "Transient Temperature Distribution in Inertia Welding of Steels", *Welding Journal*, Vol. 49 (9), Sept. 1970, Research Suppl., pp. 419-s to 426-s.

11. Box, G. E. P., "The Exploration and Exploitation of Response Surface: Some General Considerations and Examples", Biometrics, Mar. 1954, pp. 16-60.

12. Wang, K. K., and Rasmussen, G., "Optimization of Inertia Welding Process by Response Surface Methodology", Trans. ASME, Journal of Engg. for Industry, Vol. 94, No. 4, Nov. 1972, pp. 999-1006.

13. Shah, H. M., "A Mathematical Model of Metal Transfer During the Initial Stage of Inertia Welding", unpublished M.S. Theseis, Cornell University, 1973.

14. Box, G. E. P., and Hunter, W. G., "A Useful Method for Model-Building", Technometrics, Vol. 4, No. 3, Aug. 1962, pp. 301-318.

15. Philbert, J., *"X-Ray Optics and X-Ray Microanalysis"*, Pattee et al, ed., Academic Press, 1963, pp. 379-392.

16. Hansen, M., *"Constitution of Binary Alloys"*, McGraw-Hill, 1958.